Research Article

Nano Research
2020, 13(7): 1908–1911

ISSN 1998-0124 CN 11-5974/O4
https://doi.org/10.1007/s12274-020-2685-0

Superatomic Au_{13} clusters ligated by different N-heterocyclic carbenes and their ligand-dependent catalysis, photoluminescence, and proton sensitivity

Hui Shen[1], Sijin Xiang[1], Zhen Xu[1], Chen Liu[2], Xihua Li[1], Cunfa Sun[1], Shuichao Lin[1], Boon K. Teo[1], and Nanfeng Zheng[1] (✉)

[1] *State Key Laboratory for Physical Chemistry of Solid Surfaces, Collaborative Innovation Center of Chemistry for Energy Materials, National & Local Joint Engineering Research Center of Preparation Technology of Nanomaterials, College of Chemistry and Chemical Engineering, Xiamen University, Xiamen 361005, China*

[2] *School of Pharmaceutical Science, Xiamen University, Xiamen 361002, China*

Received: 10 November 2019 / **Revised:** 26 January 2020 / **Accepted:** 27 January 2020

ABSTRACT

We report herein a class of superatomic Au_{13} clusters stabilized by different N-heterocyclic carbenes (NHCs). The clusters show diverse metal surface structures, properties and functions as exemplified by: (1) the first anionic Au_{13} cluster $[Au_{13}(NHC\text{-}1)_6Br_6]^-$, which has bulky NHC-1 ligands that lead to a rather open metal surface contributing to its high catalytic activity; (2) the tricationic cluster $[Au_{13}(NHC\text{-}2)_5Br_2]^{3+}$ which has bidentate, benzyl-rich NHC-2 ligands that make it ultra-stable and highly-luminescent, suitable for bio-imaging; and (3) by bearing two pyridyl groups on NHC-3, the dicationic cluster $[Au_{13}(NHC\text{-}3)_9Cl_3]^{2+}$ exhibits reversible and stable visible absorption and solubility responses to protonation/deprotonation cycles, making it a potential pH sensor (NHC-1 = 1,3-diisopropylbenzimidazolin-2-ylidene; NHC-2 = 1,3-bis(1-benzyl-1H-benzimidazol-1-ium-3-yl)propane; NHC-3 = 1,3-bis(picolyl)benzimidazolin-2-ylidene). The study nicely demonstrates the importance of ligands in designing metal nanoclusters with desired functionalities.

KEYWORDS

carbene ligands, gold nanocluster, catalysis, luminescence, Au_{13}

1 Introduction

Atomically precise, ligand-protected metal nanoclusters (NCs) are important [1–3] in applications such as bio-imaging [4, 5], chemical sensing [6, 7], catalysis [8–11], and nanomedicine [12, 13]. The properties of metal NCs are primarily determined by their compositions and structures, within which metal configuration, ligand type and disposition, and metal-ligand interface are key factors [14]. To introduce functional diversity to a given metal NC, ligand exchange strategy may be employed [15, 16], but this methodology can be limited due to incomplete ligand exchange and the difficulty in mapping the exchange sites [17]. Recent studies by Workentin et al. demonstrated an efficient strategy to multi-functionalize Au_{25} by introducing a clickable azide to thiol ligand, whose metal-organic interfacial structure can not be significantly tuned [18].

N-heterocyclic carbenes (NHCs) have recently emerged as a new class of ligands in the filed of gold NCs [19, 20]. In particular, the work by Crudden and co-workers demonstrated a pioneer work on imparting NHCs on Au NCs via ligand-substituent strategy, yielding the first single-crystal structure of Au NC with an N-heterocyclic carbene ligand [21]. Very recently, Au_{13} and Au_{25} stabilized by NHC and halides have also been reported by Crudden and Zheng groups, respectively [22, 23]. In these works, it was found that NHC-stabilized Au NCs are highly stable, providing us a perfect platform for their further functionalization. A further attractive feature of NHCs is that there is comparative ease to prepare and study various structurally diverse analogues [24–26]. Especially, the N-substituents situated adjacent to carbene center have significant influence on their electronic and stereochemical environments. The dependence and sensitivity of the structure of the resulting cluster on the nitrogen-substituents allow fine-tuning of their properties for specific applications.

Herein we report the syntheses, structures, and properties of three clusters Au_{13} protected by NHCs and halide ligands. The first cluster, characterized as $[Au_{13}(NHC\text{-}1)_6Br_6]^-$ (1, shown in Fig. 1(d)), was synthesized with 1,3-diisopropylbenzimidazolin-2-ylidene (NHC-1) which has two bulky wing-tip iso-propyl groups (Fig. 1(a)). It is the first anionic Au_{13} cluster known to date. Cluster 1 has a wide open surface and is catalytically active. The second cluster is a trication, formulated as $[Au_{13}(NHC\text{-}2)_5Br_2]^{3+}$ (2, Fig. 1(e)), was prepared by using a bidentate carbene ligand 1,3-bis(1-benzyl-1H-benzimidazol-1-ium-3-yl)propane (NHC-2) (Fig. 1(b)). Cluster 2 is ultra-stable and highly luminescent. The third cluster is the dicationic $[Au_{13}(NHC\text{-}3)_9Cl_3]^{2+}$ (3, Fig. 1(f)) protected by 1,3-bis(picolyl) benzimidazolin-2-ylidene (NHC-3) (Fig. 1(c)) functionalized

Address correspondence to nfzheng@xmu.edu.cn

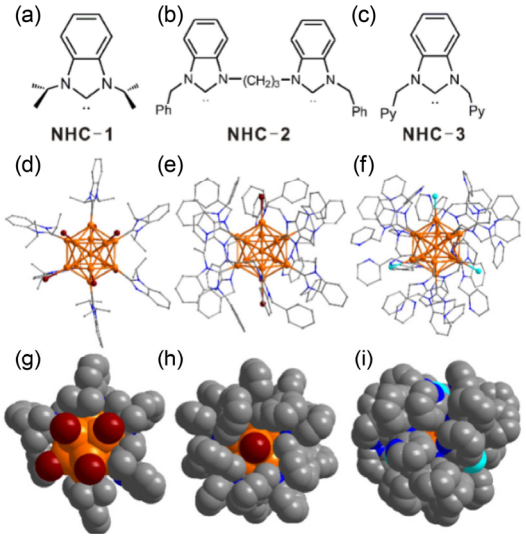

Figure 1 Molecular structure of NHCs used in this work (a)–(c); atomic structure of three Au_{13} superatoms $[Au_{13}(NHC\text{-}1)_6Br_6]^-$ (1), $[Au_{13}(NHC\text{-}2)_5Br_2]^{3+}$ (2), and $[Au_{13}(NHC\text{-}3)_9Cl_3]^{2+}$ (3), respectively (d)–(f); packing structure of the three superatoms, respectively (g)–(i). Color legend: orange, Au; red, Br; turquoise, Cl; blue, N; gray, C and H atoms are omitted for clarity.

with pyridine-bearing wing-tips. Cluster 3 exhibits reversible visible absorption and solubility response to protonation/deprotonation. Our findings offer promise for producing metal nanoclusters with outstanding performance in diverse fields such as biomaterials, catalysis, sensors, etc.

2 Results and discussion

2.1 Synthesis, characterization and atomic strucure

The detailed synthesis of ligands, gold precursors and clusters are provided in the Electronic Supplementary Material (ESM) (Schemes S1–S3 and Fig. S1–S9). In brief, alkylation of benzimidazole with haloalkanes affords NHCs [27], which after reacting with Au salts, give NHC-Au complexes [28]. The reduction of the gold precusors in a one-pot synthesis afforded three Au_{13} clusters described below.

All three clusters were characterized by single-crystal X-ray crystallography, revealing the complete formulations as $[^i\text{Pr-bimyH}][Au_{13}(NHC\text{-}1)_6Br_6]$ for 1, $[Au_{13}(NHC\text{-}2)_5Br_2]Br_3$ for 2, and $[Au_{13}(NHC\text{-}3)_9Cl_3](SbF_6)_2$ for 3 (cf. Figs. 1(d)–1(f)). Interestingly, there is a $[^i\text{Pr-bimyH}]^+$ cation co-crystallized with cluster 1 (as counter cation). Unexpectedly, clusters 1, 2, and 3 bear different overall charges of −1, +3, and +2, respectively, as a result of the NHC ligands used. 1, 2 and 3 crystallize in the centrosymmetric $P2_1/n$, $P2_1/c$ and $P2_1/c$ space groups (Table S1 in the ESM) whose unit cells contain 2, 4, and 4 clusters (Figs. S10 and S11 in the ESM), respectively.

The metal core of 1, 2, or 3 is a centered icosahedron, which is capped by both NHCs and halides. Detailed structure information of clusters 1–3 are summarized in Table S2 in the ESM. Including the carbine and halide atoms, cluster 1 has no symmetry elements (Fig. S12 in the ESM). Cluster 2 belongs to idealized D_{5d} and cluster 3 conforms to pseudo C_3 symmetry (Figs. S13 and S14 in the ESM). Based on the formulas and Jellium model, all three clusters are 8-electron superatoms [29] and are expected to be stable.

The co-crystallization of a $[^i\text{Pr-bimyH}]^+$ cation for each $[Au_{13}(NHC\text{-}1)_6Br_6]^-$ in 1 was confirmed by ^{1}H NMR (Fig. S15), indicating the negative charge of 1. The molecular compositions of 2 and 3 were independently confirmed by electrospray ionization mass measurement (ESI-MS) (Fig. S16 in the ESM). Perfect agreement between simulated isotopic pattern and experimental spectrum confirms their composition. Ultraviolet/visible (UV/Vis) spectra of title superatoms are similar, with two main peaks at ~ 410 and ~ 520 nm (Fig. S17 in the ESM).

2.2 Bulky NHC endows cluster 1 with open and catalytically active surface

As stated previously, cluster 1, with its bulky NHC-1 ligands (bulky ^{i}Pr nitrogen-substituents), has a rather open metal surface (cf. Figs. 1(a), 1(d) and 1(g)) and may be catalytically active. Indeed, it can catalyze hydrochlorination of phenylacetylene [30, 31]. The catalytic reaction was conducted by adding 5% mmol activated carbon (XC-72)-supported cluster 1 (based on Au) to a solution of phenylacetylene in 1,2-dichloroethane and bubbling HCl gas into the solution. As illustrated in Fig. 2(a), cluster 1 displayed an extremely high activity in hydrochlorination of phenylacetylene to (1-chlorovinyl)benzene at 25 °C as its conversion close to 100% after 4 h. Moreover, the catalyst displayed an excellent stability as multiple runs of the reaction afforded the desired product with almost the same reaction reactivity (Fig. 2(b)). We also compared the UV/Vis spectroscopic fingerprints and transmission electron microscopy (TEM) images of the fresh and used catalysts, no change was observed in spectral features and particle size, indicating that Au nanoclusters were intact during the catalysis reaction (Figs. S18 and S19 in the ESM). We attribute the observed excellent catalysis ability of 1 to its sterically open halide sites. In contrast, cluster 2 (to be discussed next) and cluster 3 exhibit no reactivity, which may be due to its nearly full surface coverage by ligands.

2.3 Bidentate NHC-2 makes cluster 2 ultra-stable, highly-luminescent and applicable for bio-imaging

Based on the 8-electron count of superatom, cluster 2 is expected to be rather stable. We were, however, surprised by its ultra-high stability. As shown in Fig. S20 in the ESM, the UV/Vis spectrum of 2 showed no discernible change after 12 h treatment with various temperatures (i.e., 100 and −70 °C), redox conditions (i.e., H_2O_2, $NaBH_4$), a wide range of pH from 1 to 11, and bio-related media. The ultra-stability of 2 was also confirmed by tracking its fluorescence spectra under above-mentioned conditions (Fig. S21 in the ESM). The most amazing observation is that 2 can even survive up to 6 min when treated with freshly prepared aqua regia (Fig. S22 in the ESM).

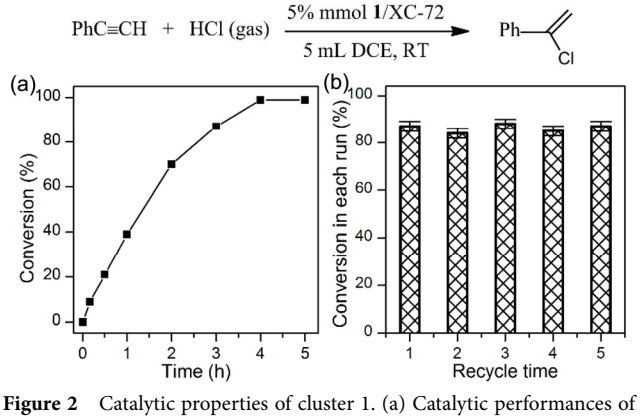

Figure 2 Catalytic properties of cluster 1. (a) Catalytic performances of 5% mmol 1/XC-72 recorded at different reaction time points for the hydrochlorination of phenylacetylene in the first run. (b) Recyclability of XC-72 supported 1 in term of activity (the conversion was calculated based on the catalysis reaction time of 3 h). Reaction conditions: 25 °C (RT), 1,2-dichloroethane (DCE) as solvent, 5% mmol catalyst (based on Au), naphthalene as internal standard, yield was determined by ^{1}H NMR.

In addition to its ultra-stability, 2 exhibits strong luminescence in both solid and solution form under UV light (Fig. S23(b) in the ESM). Upon excitation at 420 nm, 2 exhibits a prominent peak at 650 nm with a high quantum yield of 15% (Fig. 3(a), red trace) and luminescence decay time of 2.4 μs (Fig. 3(b)). We believe the photoluminescence can be attributed to the intra-cluster π···π, C–H···π and C–H···Au interactions between neighboring NHC ligands as well as between NHC ligands and select gold atoms (Fig. S24 in the ESM), which significantly restrict the movement of the planar NHC ligands on the surface of the cluster to inhibit the non-radiative radiation. In comparison, cluster 1 with open surface structure is barely photoluminescent (Fig. S23(a) in the ESM). With also bulky ligands stabilizing its surface, cluster 3 exhibits a similar photoluminescent behavior to that of 2. But the quantum yield of 3 is 7.5% (Fig. 3(c)). Its luminescence decay time is 1.2 μs, also shorter than that of 2 (Fig. 3(d)).

Inspired by encouraging results obtained through a series of stability tests and its outstanding photoluminescence property, we further investigated the potential application of 2 in cell imaging. Human cervico carcinoma cell (HeLa) line was chosen to evaluate the ability of 2 to light up affected part of the cell. The standard 3-(4,5-dimethylthiazol-2)-2,5-diphenyltetrazole bromide (MTT) assay suggested that 20 μM of 2 in dimethyl sulfoxide (DMSO)/Dulbecco's modified Eagle's medium (DMEM) (1:99) did not induce obvious cytotoxicity to HeLa (Fig. S25 in the ESM). Therefore, 10 μM in DMSO/DMEM (1:99) was administered to HeLa cells of which at least 90% remained viable for the following confocal fluorescence imaging. To help position live cells in dark field, we also utilized commercial staining agent Mito-Tracker Green® which confers mitochondria a green color under 488 nm laser irradiation. It is clearly depicted in the overlay image (Fig. 4(e)) that prominent red signal attaches onto the cell membrane. Meanwhile, we also observed that 2 suffered from non-substantial cellular internalization due to relatively long incubation time (Fig. 4). Confocal fluorescence images were captured at different incubation periods (Fig. S26 in the ESM). The brightness of emission originated from cluster 2 was revealed to become significant at 4 h and keep beyond 12 h. Moreover, the hydrodynamic size, zeta potential and UV/Vis spectroscopic measurements also suggested no obvious aggregation of cluster 2 in physiological environment (i.e. phosphate buffered saline (PBS), culture media), and under strong irradiation of Xe lamp for 12 h (Figs. S27 and 28 in the ESM), making cluster 2 promising for biological applications.

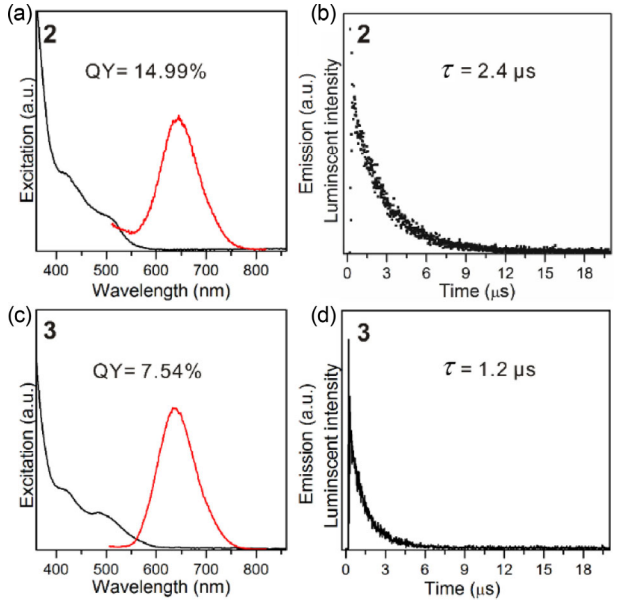

Figure 3 (a) and (c) UV/Vis (black) and emission (red, excited at 420 nm) spectra of 2 and 3. (b) and (d) Luminescent decay curve of 2 and 3 at room temperature.

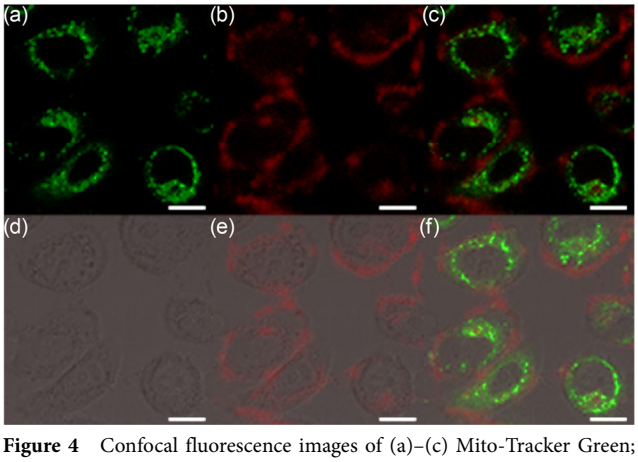

Figure 4 Confocal fluorescence images of (a)–(c) Mito-Tracker Green; cluster 2; overlay in dark field. (d)–(f) Hela cells; cluster 2; overlay in bright field. Scale bar = 20 μm.

2.4 Pyridyl-bearing NHC-3 functions the superatom reversible visible absorption and solubility responses to protonation/deprotonation events

Owing to the basicity of the pyridyl substituents on the two N atoms ortho to the carbene atom, cluster 3 exhibits optical and solubility responses to protonation/deprotonation. In detail, when 3 was dissolved in dichloromethane and treated with hydrochloric acid, it was readily transferred into aqua phase (Fig. 5, inset). The absorption band of 3 was shifted from 408 to 415 nm (Fig. 5), suggesting that the formation of a cationic charge at the distal pyridyl nitrogen would influence the electronic and physical properties of the Au_{13} moieties. Note that these protonation/deprotonation cycles are completely reversible and reproducible. The spectrum of the protonated form of 3 was reverted to its original pattern upon neutralization of the solution by the addition of a base such as $NaHCO_3$ (Fig. 5), suggesting that this system may be used as a pH indicator.

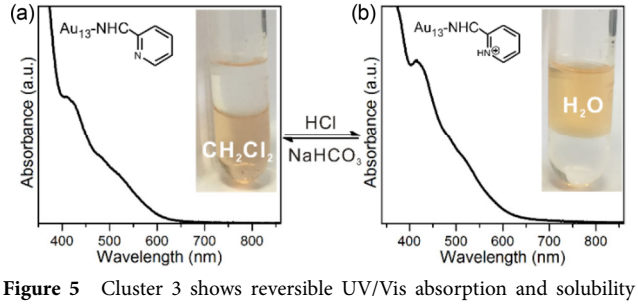

Figure 5 Cluster 3 shows reversible UV/Vis absorption and solubility responses to protonation/deprotonation events.

3 Conclusion

In summary, three centered icosahedral Au_{13} clusters, 1, 2, and 3, protected by different N-heterocyclic carbene and halide ligands, were prepared and structurally characterized. It was demonstrated that for a given metal framework, modification of N-heterocyclic carbenes is an efficient strategy to tune its surface structure, physic-chemical properties, and tailorable for specific applications. It was demonstrated that (1) cluster 1 has bulky NHC-1 ligands which leads to a rather open metal surface contributing to its high catalytic activity; (2) cluster 2

has bidentate, benzyl-rich NHC-2 ligands that makes it ultra-stable and highly-luminescent, suitable for bio-imaging; and (3) by bearing two pyridyl groups on the NHC-3 ligands, cluster 3 exhibits reversible and stable visible absorption and solubility responses to protonation/deprotonation cycles, making it a potential pH sensor. Other functions, such as magnetism, chirality, and semi-conductivity, of NHC-ligated metal clusters are under development in our laboratory.

Acknowledgements

We thank the National Key R&D Program of China (No. 2017YFA0207304), the National Nautural Science Foundation of China (Nos. 21890752, 21731005, 21802109, and 21721001), and the fundamental research funds for central universities (No. 20720190043) for financial support.

Electronic Supplementary Material: Supplementary material (detailed synthesis and characterizations including UV/Vis and emission spectra, cell toxicity, bioimaging data, and cif files for the three clusters) is available in the online version of this article at https://doi.org/10.1007/s12274-020-2685-0.

References

[1] Jin, R. C.; Zeng, C. J.; Zhou, M.; Chen, Y. X. Atomically precise colloidal metal nanoclusters and nanoparticles: Fundamentals and opportunities. *Chem. Rev.* **2016**, *116*, 10346–10413.

[2] Chakraborty, I.; Pradeep, T. Atomically precise clusters of noble metals: Emerging link between atoms and nanoparticles. *Chem. Rev.* **2017**, *117*, 8208–8271.

[3] Yan, J. Z.; Teo, B. K.; Zheng, N. F. Surface chemistry of atomically precise coinage-metal nanoclusters: From structural control to surface reactivity and catalysis. *Acc. Chem. Res.* **2018**, *51*, 3084–3093.

[4] Shang, L.; Azadfar, N.; Stockmar, F.; Send, W.; Trouillet, V.; Bruns, M.; Gerthsen, D.; Nienhaus, G. U. One-pot synthesis of near-infrared fluorescent gold clusters for cellular fluorescence lifetime imaging. *Small* **2011**, *7*, 2614–2620.

[5] Raut, S. L.; Fudala, R.; Rich, R.; Kokate, R. A.; Chib, R.; Gryczynski, Z.; Gryczynski, I. Long lived BSA Au clusters as a time gated intensity imaging probe. *Nanoscale* **2014**, *6*, 2594–2597.

[6] Xie, J. P.; Zheng, Y. G.; Ying, J. Y. Highly selective and ultrasensitive detection of Hg^{2+} based on fluorescence quenching of Au nanoclusters by Hg^{2+}-Au^{+} interactions. *Chem. Commun.* **2010**, *46*, 961–963.

[7] Roy, S.; Palui, G.; Banerjee, A. The as-prepared gold cluster-based fluorescent sensor for the selective detection of As^{III} ions in aqueous solution. *Nanoscale* **2012**, *4*, 2734–2740.

[8] Wang, Y.; Wan, X. K.; Ren, L. T.; Su, H. F.; Li, G.; Malola, S.; Lin, S. C.; Tang, Z. C.; Häkkinen, H.; Teo, B. K. et al. Atomically precise alkynyl-protected metal nanoclusters as a model catalyst: Observation of promoting effect of surface ligands on catalysis by metal nanoparticles. *J. Am. Chem. Soc.* **2016**, *138*, 3278–3281.

[9] Wan, X. K.; Wang, J. Q.; Nan, Z. A.; Wang, Q. M. Ligand effects in catalysis by atomically precise gold nanoclusters. *Sci. Adv.* **2017**, *3*, e1701823.

[10] Li, G.; Jin, R. C. Atomically precise gold nanoclusters as new model catalysts. *Acc. Chem. Res.* **2013**, *46*, 1749–1758.

[11] Yamazoe, S.; Koyasu, K.; Tsukuda, T. Nonscalable oxidation catalysis of gold clusters. *Acc. Chem. Res.* **2014**, *47*, 816–824.

[12] Zheng, K. Y.; Setyawati, M. I.; Leong, D. T.; Xie, J. P. Antimicrobial gold nanoclusters. *ACS Nano* **2017**, *11*, 6904–6910.

[13] Wang, Y. C.; Wang, Y.; Zhou, F. B.; Kim, P.; Xia, Y. N. Protein-protected Au clusters as a new class of nanoscale biosensor for label-free fluorescence detection of proteases. *Small* **2012**, *8*, 3769–3773.

[14] Konishi, K.; Iwasaki, M.; Shichibu, Y. Phosphine-ligated gold clusters with core+exo geometries: Unique properties and interactions at the ligand-cluster interface. *Acc. Chem. Res.* **2018**, *51*, 3125–3133.

[15] Tracy, J. B.; Crowe, M. C.; Parker, J. F.; Hampe, O.; Fields-Zinna, C. A.; Dass, A.; Murray, R. W. Electrospray ionization mass spectrometry of uniform and mixed monolayer nanoparticles: $Au_{25}[S(CH_2)_2Ph]_{18}$ and $Au_{25}[S(CH_2)_2Ph]_{18-x}(SR)_x$. *J. Am. Chem. Soc.* **2007**, *129*, 16209–16215.

[16] Dass, A.; Stevenson, A.; Dubay, G. R.; Tracy, J. B.; Murray, R. W. Nanoparticle MALDI-TOF mass spectrometry without fragmentation: $Au_{25}(SCH_2CH_2Ph)_{18}$ and mixed monolayer $Au_{25}(SCH_2CH_2Ph)_{18-x}(L)_x$. *J. Am. Chem. Soc.* **2008**, *130*, 5940–5946.

[17] Ren, L. T.; Yuan, P.; Su, H. F.; Malola, S.; Lin, S. C.; Tang, Z. C.; Teo, B. K.; Häkkinen, H.; Zheng, L. S.; Zheng, N. F. Bulky surface ligands promote surface reactivities of $[Ag_{141}X_{12}(S\text{-}Adm)_{40}]^{3+}$ (X = Cl, Br, I) nanoclusters: Models for multiple-twinned nanoparticles. *J. Am. Chem. Soc.* **2017**, *139*, 13288–13291.

[18] Gunawardene, P. N.; Corrigan, J. F.; Workentin, M. S. Golden opportunity: A clickable azide-functionalized $[Au_{25}(SR)_{18}]^{-}$ nanocluster platform for interfacial surface modifications. *J. Am. Chem. Soc.* **2019**, *141*, 11781–11785.

[19] Tang, Q.; Jiang, D. E. Comprehensive view of the ligand–gold interface from first principles. *Chem. Mater.* **2017**, *29*, 6908–6915.

[20] Muñoz-Castro, A. Potential of N-heterocyclic carbene derivatives from $Au_{13}(dppe)_5Cl_2$ gold superatoms. Evaluation of electronic, optical and chiroptical properties from relativistic DFT. *Inorg. Chem. Front.* **2019**, *6*, 2349–2358.

[21] Narouz, M. R.; Osten, K. M.; Unsworth, P. J.; Man, R. W. Y.; Salorinne, K.; Takano, S.; Tomihara, R.; Kaappa, S.; Malola, S.; Dinh, C. T. et al. N-heterocyclic carbene-functionalized magic-number gold nanoclusters. *Nat. Chem.* **2019**, *11*, 419–425.

[22] Narouz, M. R.; Takano, S.; Lummis, P. A.; Levchenko, T. I.; Nazemi, A.; Kaappa, S.; Malola, S.; Yousefalizadeh, G.; Calhoun, L. A.; Stamplecoskie, K. G. et al. Robust, highly luminescent Au_{13} superatoms protected by N-heterocyclic carbenes. *J. Am. Chem. Soc.* **2019**, *141*, 14997–15002.

[23] Shen, H.; Deng, G. C.; Kaappa, S.; Tan, T. D.; Han, Y. Z.; Malola, S.; Lin, S. C.; Teo, B. K.; Häkkinen, H.; Zheng, N. F. Highly robust but surface-active: N-heterocyclic carbene-stabilized Au_{25} nanocluster. *Angew. Chem., Int. Ed.* **2019**, *58*, 17731–17735.

[24] Smith, C. A.; Narouz, M. R.; Lummis, P. A.; Singh, I.; Nazemi, A.; Li, C. H.; Crudden, C. M. N-Heterocyclic carbenes in materials chemistry. *Chem. Rev.* **2019**, *119*, 4986–5056.

[25] Zhukhovitskiy, A. V.; MacLeod, M. J.; Johnson, J. A. Carbene ligands in surface chemistry: From stabilization of discrete elemental allotropes to modification of nanoscale and bulk substrates. *Chem. Rev.* **2015**, *115*, 11503–11532.

[26] Mercs, L.; Albrecht, M. Beyond catalysis: N-Heterocyclic carbene complexes as components for medicinal, luminescent, and functional materials applications. *Chem. Soc. Rev.* **2010**, *39*, 1903–1912.

[27] Crudden, C. M.; Horton, J. H.; Ebralidze, I. I.; Zenkina, O. V.; McLean, A. B.; Drevniok, B.; She, Z.; Kraatz, H. B.; Mosey, N. J.; Seki, T. et al. Ultra stable self-assembled monolayers of N-heterocyclic carbenes on gold. *Nat. Chem.* **2014**, *6*, 409–414.

[28] Collado, A.; Gómez-Suárez, A.; Martin, A. R.; Slawin, A. M. Z.; Nolan, S. P. Straightforward synthesis of [Au(NHC)X] (NHC = N-heterocyclic carbene, X = Cl, Br, I) complexes. *Chem. Commun.* **2013**, *49*, 5541–5543.

[29] Walter, M.; Akola, J.; Lopez-Acevedo, O.; Jadzinsky, P. D.; Calero, G.; Ackerson, C. J.; Whetten, R. L.; Gronbeck, H.; Hakkinen, H. A unified view of ligand-protected gold clusters as superatom complexes. *Proc. Natl. Acad. Sci. USA* **2008**, *105*, 9157–9162.

[30] Gribble, G. W. Naturally occurring organohalogen compounds. *Acc. Chem. Res.* **1998**, *31*, 141–152.

[31] Petrone, D. A.; Ye, J. T.; Lautens, M. Modern transition-metal-catalyzed carbon-halogen bond formation. *Chem. Rev.* **2016**, *116*, 8003–8104.